Noise Floor Removal via Phase Correction of Complex Diffusion-Weighted Images: Influence on DTI and q-space Metrics

Marco Pizzolato[1⋆], Rutger Fick[1], Timothé Boutelier[2], and Rachid Deriche[1]

[1] Université Côte d'Azur, Inria, France
[2] Olea Medical, La Ciotat, France

Abstract. The non-Gaussian noise distribution in magnitude Diffusion-Weighted Images (DWIs) can severely affect the estimation and reconstruction of the true diffusion signal. As a consequence, also the estimated diffusion metrics can be biased. We study the effect of phase correction, a procedure that re-establishes the Gaussianity of the noise distribution in DWIs by taking into account the corresponding phase images. We quantify the debiasing effects of phase correction in terms of diffusion signal estimation and calculated metrics. We perform *in silico* experiments based on a MGH Human Connectome Project dataset and on a digital phantom, accounting for different acquisition schemes, diffusion-weightings, signal to noise ratios, and for metrics based on Diffusion Tensor Imaging and on Mean Apparent Propagator Magnetic Resonance Imaging, i.e. q-space metrics. We show that phase correction is still a challenge, but also an effective tool to debias the estimation of diffusion signal and metrics from DWIs, especially at high b-values.

1 Introduction

Diffusion-Weighted Magnetic Resonance Imaging (DW-MRI) is inherently a low Signal to Noise Ratio (SNR) technique [1]. More diffusion weighting – globally encoded by a larger b-value – leads to lower signal intensities and consequently to a poorer SNR. In such a low SNR regime, the magnitude of the complex DW signal can be dominated by a bias, namely noise floor, which is due to the non-Gaussian distribution of the noise. This generally falls within the non-central χ^2 family, depending on the adopted MR acquisition strategy (number of coils, multi-coil reconstruction, acceleration, etc.) [2]. However, some diffusion MRI techniques require the acquisition of Diffusion-Weighted Images (DWIs) at relatively high b-values [3–5], where the Noise Floor affects the signal estimation and consequent parameter calculations. A strategy for removing the Noise Floor from the magnitude DWIs, is *phase correction* [6]. This method consists on estimating the true phase from the complex DWIs to transfer the image content – which is split between real (rDWI) and imaginary (iDWI) parts – into the

⋆ The author expresses his thanks to Olea Medical and the Provence-Alpes-Côte d'Azur (PACA) Regional Council for providing grant and support for this work.

real part only, such that the rDWIs contain the signal corrupted by Gaussian distributed noise. In this work, we quantify the influence of phase correction in terms of unbiased signal estimation and reconstruction. In the latter case, we focus on two popular signal-driven representations of the diffusion process, such as Diffusion Tensor Imaging (DTI) [7] and Mean Apparent Propagator Magnetic Resonance Imaging (MAP) [3], and we quantify the effects of phase correction on the corresponding scalar parameters. We present *in silico* experiments based on a MGH Human Connectome Project (HCP) dataset and on a digital phantom.

The noise floor causes a signal overestimation that is more important at high b-values and when diffusion is less restricted, i.e. when the signal is low. This introduces a bias that leads to the distortion of the estimated quantitative diffusion metrics, such as the underestimation of the Apparent Diffusion Coefficient (ADC) in DTI [1]. This affects the principal diffusivity (PD), i.e. the amplitude of the tensor's eigenvector aligned to the least restricted direction, which is underestimated. Similar considerations hold for other DTI metrics, such as the fractional anisotropy (FA). Moreover, since MAP signal reconstruction typically requires high b-values, we also expect some of the derived q-space metrics to be biased. In this scenario, phase correction is a promising tool to calculate unbiased metrics.

Phase correction exploits the phase images associated with the magnitude DWIs. Some advantages of using the phase of the DW signal, to perform a reconstruction directly in the complex domain, have been previously reported [8], while assuming phase coherence among q-space samples. However, in actual DW-MRI acquisitions the phase images are subject shot-wise variations that are mainly dominated by movements, cardiac pulsation, blood circulation or field inhomogeneity. Thus, coherent phase contributions related to the diffusion process, e.g., asymmetries due to tissue configurations or experimental setups [9–11], are hardly observable and are not explicitly accounted in noise floor removal via phase correction.

Recent phase corrections for noise floor removal consist on filtering the real and imaginary images, i.e. the rDWI and iDWI, to obtain a low-frequency version of the DWI's phase, which is used to complex-rotate the rDWI and iDWI such that former contains the signal plus Gaussian distributed noise, and the latter only noise (which will be discarded). The filtering is typically performed via a convolution procedure [12, 13] or total variation [14]. However, the correct estimation of the low-frequency phase depends on the correct choice of the convolution kernel (and its size) or regularization parameter. Therefore, the effectiveness of phase correction on signal debiasing and diffusion parameters estimation, such as DTI and MAP metrics, needs to be assessed.

In this work, we implement a phase correction procedure based on total variation [14]. We first apply it to *in silico* complex DWIs, created by processing a HCP dataset, in order to assess the effectiveness of the phase correction in a realistic scenario, for different diffusion weightings, i.e. b-values, and SNRs. At the same time, we assess the amount of noise floor bias in typical magnitude DWIs (|DWI|) – based on signal probability distribution metrics – and the correspond-

ing improvement after phase correction. In second place, we asses the influence of phase correction on DTI and q-space metrics. Particularly, we apply phase correction to complex DWIs produced by using a modified version of Phantomαs [15], while accounting for different total variation regularizations and for typical acquisition setups, i.e. single-shell at $b \in \{1000, 2000, 3000\}$ s/mm^2 (DTI), and multi-shell (DTI, MAP).

2 Methods

In this section, we describe the implemented phase correction procedure, and illustrate the generation of the data used for the experiments, such as the acquisition setup, the generation of a synthetic phase, and the SNR convention.

The phase correction takes into account a complex DWI

$$\mathrm{DWI}_{xy} = \mathrm{rDWI}_{xy} + j \cdot \mathrm{iDWI}_{xy} \tag{1}$$

where x and y represent the pixel coordinates, r and i indicate the real and imaginary parts, and j is the imaginary unit. If $\widehat{\angle DWI}_{xy}$ is a good estimation of the phase, then the phase-corrected image is obtained via complex rotation

$$\mathrm{DWI}^{pc}_{xy} = |\mathrm{DWI}|_{xy} e^{j\left(\angle \mathrm{DWI}_{xy} - \widehat{\angle \mathrm{DWI}}_{xy}\right)} \tag{2}$$

where $\angle \mathrm{DWI}_{xy}$ and $|\mathrm{DWI}|_{xy}$ are the original noisy phase and magnitude. The real part of the phase-corrected complex DWI, $\Re(\mathrm{DWI}^{pc}_{xy})$, contains the signal (tissue contrast) plus Gaussian distributed noise, whereas the imaginary part, $\Im(\mathrm{DWI}^{pc}_{xy})$, only contains noise. Henceforth, any classical diffusion modeling and reconstruction taking into account additive Gaussian noise can be performed on $\Re(\mathrm{DWI}^{pc}_{xy})$, where the noise floor is absent.

The effectiveness of phase correction clearly depends on the quality of the phase estimation. In this work we implement a total variation method, known to better preserve discontinuities in the images [14]. Particularly, for each image $u_0 \in \{\mathrm{rDWI}_{xy}, \mathrm{iDWI}_{xy}\}$ defined on coordinates $x \in X, y \in Y$, we find the image u such that it is the minimizer of

$$\inf_u \lambda \int_{X,Y} (u_0 - u)^2 dxdy + \int_{X,Y} |\nabla u| dxdy \tag{3}$$

where λ is the regularization parameter expressing the attachment to the data. The estimates of rDWI_{xy} and iDWI_{xy} obtained with eq. (3) are then used to compute $\widehat{\angle \mathrm{DWI}}_{xy}$ to perform the complex rotation in eq. (2).

2.1 Simulation and Diffusion Signal Reconstruction

The complex DWIs have in all cases been created by generating a synthetic phase image, Φ_{xy}, associated with a magnitude image, M_{xy}. The phase images

are created in order to mimic the outcome of subject movements. We assume a bi-dimensional sinusoidal wave oriented along the direction $\mathbf{v} = (v_x, v_y)$ with frequencies f_x, f_y and initial shifts ϕ_x, ϕ_y

$$\Phi(x,y) = \pi \cdot sin\left(2\pi \frac{v_x}{||\mathbf{v}||} f_x \frac{x}{w_x} + \phi_x + 2\pi \frac{v_y}{||\mathbf{v}||} f_y \frac{y}{w_y} + \phi_y\right) \tag{4}$$

where w_x, w_y are scale parameters, i.e. in this case the width of the image along the corresponding direction ($w_x = card(X)$, $w_y = card(Y)$). Eventually, constant phase patches are added. Assuming to have the ground-truth images of magnitude M_{xy} and phase Φ_{xy}, the latter resulting from eq. (4), then

$$\begin{aligned} \text{rDWI}_{xy} &= M_{xy} \cdot cos(\Phi_{xy}) + \eta^r_{xy} \\ \text{iDWI}_{xy} &= M_{xy} \cdot sin(\Phi_{xy}) + \eta^i_{xy} \end{aligned} \tag{5}$$

where $\eta^r_{xy}, \eta^i_{xy} \in N(0, \sigma^2)$. The noise is added with a value of σ calculated according to the DW-MRI convention $\sigma = \left(card[\rho(X \times Y)]^{-1} \sum_{x,y} \rho(x,y) M^{b=0}_{xy}\right) / \text{SNR}_0$, where SNR_0 is defined on the magnitude image without diffusion weighting $M^{b=0}_{xy}$, and $\rho \in \{0,1\}$ is a mask defined on the pairs (x,y), e.g., a mask of the tissue-related signal like the brain mask. The Rician magnitude $|\text{DWI}|_{xy}$ and the phase $\underline{/\text{DWI}}_{xy}$ are calculated from the real and imaginary parts in eq. (5).

The data used for the experiments is a HCP brain dataset corrected for eddy currents where we selected DWIs of interest for $b \in [0, 1000, 3000]$ s/mm^2. Other experiments use Phantomαs [15] to obtain the ground-truth magnitude images, M_{xy}. This software requires input with a geometrical description of tissue structures and fiber bundles. We used the well known geometry produced for the HARDI reconstruction challenge 2013[3]. We generated DWIs for a 3-shells scheme with $b \in \{1000, 2000, 3000\}$ s/mm^2, 51 samples *per* shell, with samples uniformly distributed within and among shells [16].

The phase-corrected real DWIs can contain negative values: the noise is zero-mean Gaussian and the noise floor is absent. Therefore, the DTI reconstruction is performed non-linearly forcing signal positivity, and MAP is performed with Laplacian regularization imposing positivity on the recovered Ensemble Average Propagator [17].

3 Experiments and Results

We perform three experiments with two objectives: first, quantifying the effect of phase correction on signal debiasing, by processing real data from a HCP dataset; second, assessing the debiasing on diffusion metrics, calculated with DTI and MAP reconstructions, on a digital dataset generated for typical scenarios such as DTI at b-value 1000, 2000, 3000 s/mm^2 and DTI and MAP multi-shell.

[3] `http://hardi.epfl.ch/static/events/2013_ISBI/`,`https://github.com/ecaruyer/phantomas/blob/master/examples/isbi_challenge_2013.txt`

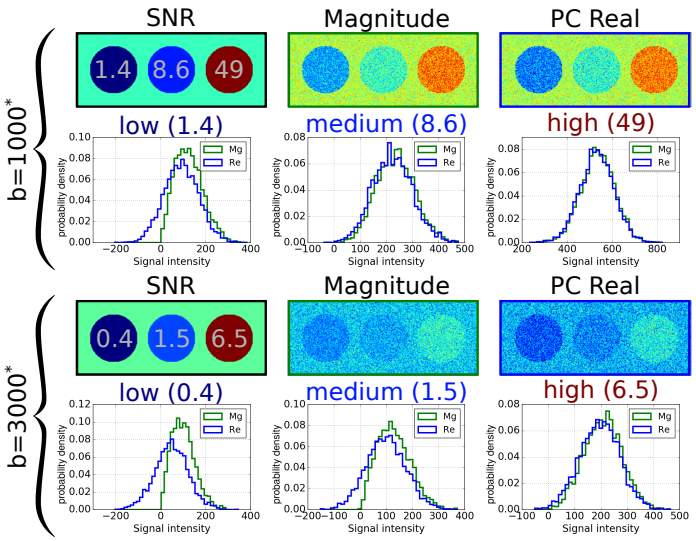

Fig. 1. The signal contrast and distributions for synthetic complex DWIs, at $b = 1000, 3000\ s/mm^2$, created from clustering a real HCP dataset ($\text{SNR}_0 = 10$). In the rectangular frames from left to right: the SNR map, the Rician magnitude (Mg) and the phase-corrected estimated real image (Re). Below, the histograms of the signal intensities corresponding to the circles with low, medium, and high signal/SNR, for Mg (green) and Re (blue). Background SNR: 21.5 for $b = 1000\ s/mm^2$ and 3.2 for $b = 1000\ s/mm^2$. *: s/mm^2.

In the *first experiment*, we clustered a HCP dataset to obtain typical signal values at b-value 1000 and 3000 s/mm^2. Particularly, for each b-value we applied k-means to divide the signal of the DWIs – accounting for all the gradient directions – into 4 clusters. We used the centroid of each cluster to define respectively background, low, medium, and high mean signal values. Based on these, we created a ground-truth synthetic magnitude image – M_{xy} in eq. (5) – composed of three circles each containing, from left to right, low, medium and high signal respectively. Outside the circles we added background signal. A synthetic phase was generated and the noisy complex DWI was created. After calculating the average $b = 0$ signal ($S(0)_{avg} = 758\,a.u.$) in the HCP dataset, noise was added as in eq. (5) in low SNR regime: $\text{SNR}_0 = 10$. Figure 1 shows, for each b-value, the noisy magnitude $|\text{DWI}|_{xy}$ and the estimated phase-corrected real part $\Re(\text{DWI}^{pc}_{xy})$ (λ set to 0.75 after visual inspection). In addition, an effective SNR map is present along with histograms of the magnitude and phase-corrected real signals for each circle. We conclude that in both cases the phase-corrected real image presents more contrast with the background compared to the magnitude. This is more evident at low SNR values – left circle at $b = 1000\ s/mm^2$, left and central circles at $b = 3000\ s/mm^2$ – that are more likely with high b-values. The $\Re(\text{DWI}^{pc}_{xy})$ shows darker colors, i.e. lower signal intensities, as it is highlighted by the histograms: the magnitude (green line) has a Rician distribution for low

SNRs (typically below SNR = 5) whereas the estimated real part (blue line) always shows a Gaussian distribution, thus including negative signal intensities. We point out that since this is an experiment grounded on real data, the centroid of the clusters – especially at low signal values – are based on Rician data and might overestimate the actual (noise-free) ones. This means that the Rician bias in histograms (green line) might be an underestimation of the true one.

In the *second experiment*, we use the HCP dataset to create a mean ground-truth magnitude DWI, M_{xy}, in order to quantify the Rician bias, i.e. the distance from Gaussianity. We calculate the mean $b = 0$ image $S(0)_{xy}$, for a slice of interest, by averaging the 40 non-diffusion-weighted images in the dataset. Since the SNR is very high, the averaging procedure is not biased. Then, we select all the DWIs corresponding to $b = 1000\ s/mm^2$ and perform DTI to obtain the mean diffusivity map, MD_{xy}. At this point, we obtain a ground-truth magnitude DWI at any b-value by extrapolating with $M_{xy} = S(b)_{xy} = S(0)_{xy} \exp(-b \cdot \mathrm{MD}_{xy})$. Although we assume Gaussian isotropic diffusion, this phantom represents an average description of a magnitude DWI. After generating a synthetic phase image, as described in section 2, we calculate the noisy complex DWI, for each b-value, as in eq. (5). Figure 2 shows the $b = 0$ magnitude and the phase used for the phantom (left column). We then calculate the Rician magnitude $|\mathrm{DWI}|_{xy}$ and the phase-corrected real part $\Re(\mathrm{DWI}^{pc}_{xy})$ ($\lambda = 0.75$). Additionally, we calculate a magnitude image with Gaussian distributed noise $|\mathrm{DWI}|^{G}_{xy}$, by adding Gaussian noise (with the same SNR_0) to M_{xy}. This will be used as reference for Gaussianity measures. We generate 1000 noise occurrences and calculate, for each pixel of the images, the signal intensities histograms of the signal intensities (as in fig. 1). For each pixel we generate 3 histograms, each related to the Rician $|\mathrm{DWI}|_{xy}$, the phase-corrected $\Re(\mathrm{DWI}^{pc}_{xy})$ and the Gaussian $|\mathrm{DWI}|^{G}_{xy}$. The hypothesis is that, for each pixel, the phase-corrected signal distribution should be closer to that of the Gaussian magnitude image than the Rician magnitude one. As a distance from Gaussianity, we use the discrete Hellinger distance [18]

$$H(P, Q) = \frac{1}{\sqrt{2}} ||\sqrt{P} - \sqrt{Q}||_2 \tag{6}$$

where P and Q are two discrete probability distributions, and $0 \leq H(P, Q) \leq 1$ where 1 means maximum distance. In columns 2 to 4, fig. 2 shows the Hellinger distance maps from the Gaussian magnitude, for the Rician magnitude (first row) and the phase-corrected real part (second row), at b-value 1000, 2000 and 3000 s/mm^2. We see that the Rician magnitude shows more bias (higher H), especially in regions where MD is high. As expected, at higher b-values (from left to right) the signal intensity is lower and the bias occurs in a larger number of pixels. Conversely, the phase-corrected real part does not show a clear change.

In the *third experiment*, we quantify the bias on the estimated DTI and MAP metrics for the Rician magnitude, and we quantify the debiasing power of phase correction by looking at the change in the distributions of such metrics compared to the Gaussian noise case. We generate complex DWIs with Phantomαs [15] as described in section 2. For each gradient direction $\mathbf{g} = (g_x, g_y, g_z)$, the

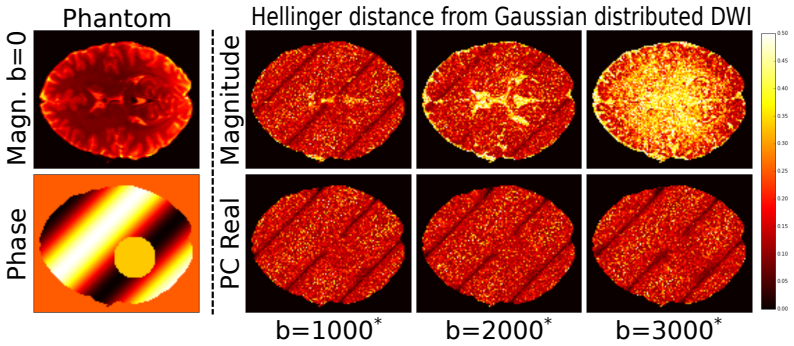

Fig. 2. The distance from Gaussianity of complex DWIs obtained by processing a HCP dataset and a synthetic phase image. In the first column the $b = 0$ magnitude image obtained from real data, and the generated phase. In the columns from the second to the fourth, the distance from the Gaussianity measured with eq. (6) for the Rician magnitude (first row) and the phase-corrected real part (second row), at different b-values (columns). Contrarily to the case of the Rician magnitude, the distance from Gaussianity remains visually unchanged as the diffusion-weighting increases. *: s/mm^2.

synthetic phase image is oriented towards $\mathbf{v} = (g_x, g_y)$ (see eq. (4)) with constant phase shifts between slices (along the z direction). Figure 3 shows the original noisy data (Rician magnitude, phase, noisy real and imaginary parts) and the one after phase correction for a reference slice ($b = 1000\ s/mm^2$). For each $\mathrm{SNR}_0 \in \{10, 20, 30\}$ we generate the Rician magnitude data and, as for the second experiment, the Gaussian DWI image to be used as reference. In this experiment we also investigate the effect of the regularization parameter λ of the total variation filtering in eq. (3). Therefore, for each SNR_0 we generate six phase-corrected datasets, for $\lambda \in \{0.25, 0.5, 0.75, 1, 2, 5\}$. For each combination of SNR_0 and type of data – Rician, Gaussian and the six phase corrections – we fit DTI with single-shell scheme at b-value 1000, 2000 and 3000 s/mm^2, and DTI and MAP with multi-shell scheme. For DTI, we calculate the mean diffusivity (MD), the principal diffusivity (PD), and the fractional anisotropy (FA). We calculate q-space metrics based on closed formulas derived for MAP. These are the return to origin (RTOP), axis (RTAP) and plane (RTPP) probabilities [3], the mean squared displacement (MSD) and the q-space inverse variance (QIV) [17]. We create a mask of voxels within fibers, based on the noise-free dataset, by considering only the voxels where $\mathrm{RTOP} \in [0.5e6, 0.7e6]$ (range chosen based on visual inspection). For each value of λ and for each calculated DTI and q-space metric, we compute the probability distribution inside the mask for the Rician, Gaussian and phase corrected data. Figure 4 illustrates the influence of the regularization parameter λ (decreasing along the rows) on the recovered metric probability distribution. The figure shows the Gaussian (red line), Rician (green line) and phase-corrected (blue line) probability distributions ($\mathrm{SNR}_0 = 10$) of PD (DTI at 1000, 2000 s/mm^2) and RTPP (MAP). The results confirm the underestimation of PD that increases with the b-value, i.e. the green histograms are

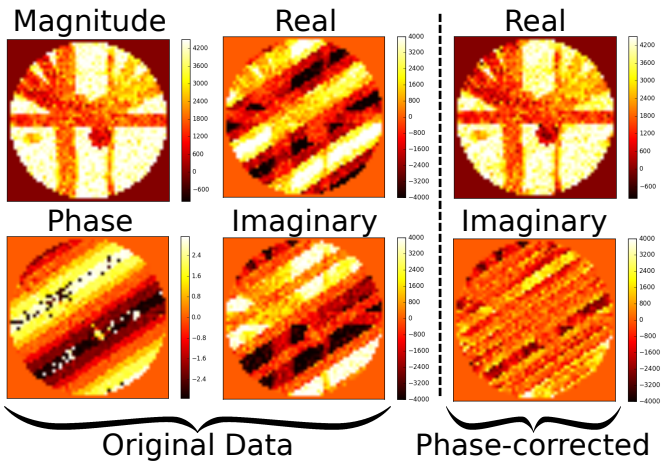

Fig. 3. A slice of data generated with the digital phantom for $\mathrm{SNR}_0 = 10$, $b = 1000$ s/mm^2. On the left: the original noisy data calculated with a ground-truth magnitude image obtained with Phantomαs [15] and a synthetic phase. On the right: the phase-corrected real and imaginary parts ($\lambda = 0.75$); the signal information is almost entirely contained in the real part, whereas the imaginary part mainly contains Gaussian noise.

left to the red ones. Consequently, also MD (see section 1) is underestimated [1]. Inverse analogous considerations hold for RTPP. We observe that λ has a great influence on the phase correction results. Particularly, a large λ implies strong attachment to data, resulting in a poor phase-correction since the estimated low-frequency phase is very similar to the original noisy one, $\widehat{\angle DWI}_{xy} \approx \underline{\angle DWI}_{xy}$ in eq. (2). Indeed, the blue histograms (phase-corrected) in the first row of fig. 4 almost entirely overlap the green ones (Rician magnitude data). As the attachment to the data decreases (from top to bottom), the blue phase-corrected histograms move towards the (red) Gaussian based distributions, visually reducing the distance from Gaussianity. As in second experiment, we quantify the distance from Gaussian metrics by using Hellinger's formula in eq. (6). Figure 5 illustrates the variation of the H distance for the phase-corrected data as function of λ, for each acquisition setup, reconstruction method (DTI, MAP) and diffusion metric. In each image, the dashed lines represent the distance value from Gaussian metrics for the metrics calculated on Rician magnitude data, whereas the solid lines report the distance for metrics calculated on phase-corrected data, which varies with λ (abscissa). Color codes indicate the SNR_0 value. We observe that phase correction leads to metric distributions that are closer to the Gaussianity (H distance close to 0) than the Rician magnitude ones, for specific ranges of λ. In general, phase correction debiases the metric distributions up to a great extent. The improvement over the Rician magnitude is clearly correlated with the combination of acquisition scheme – especially the maximum b-value – and SNR_0 as also indicated by the signal intensities experiments and illustrated in figs. 1 and 2. Indeed, at high b-values the signal is low – especially along the less

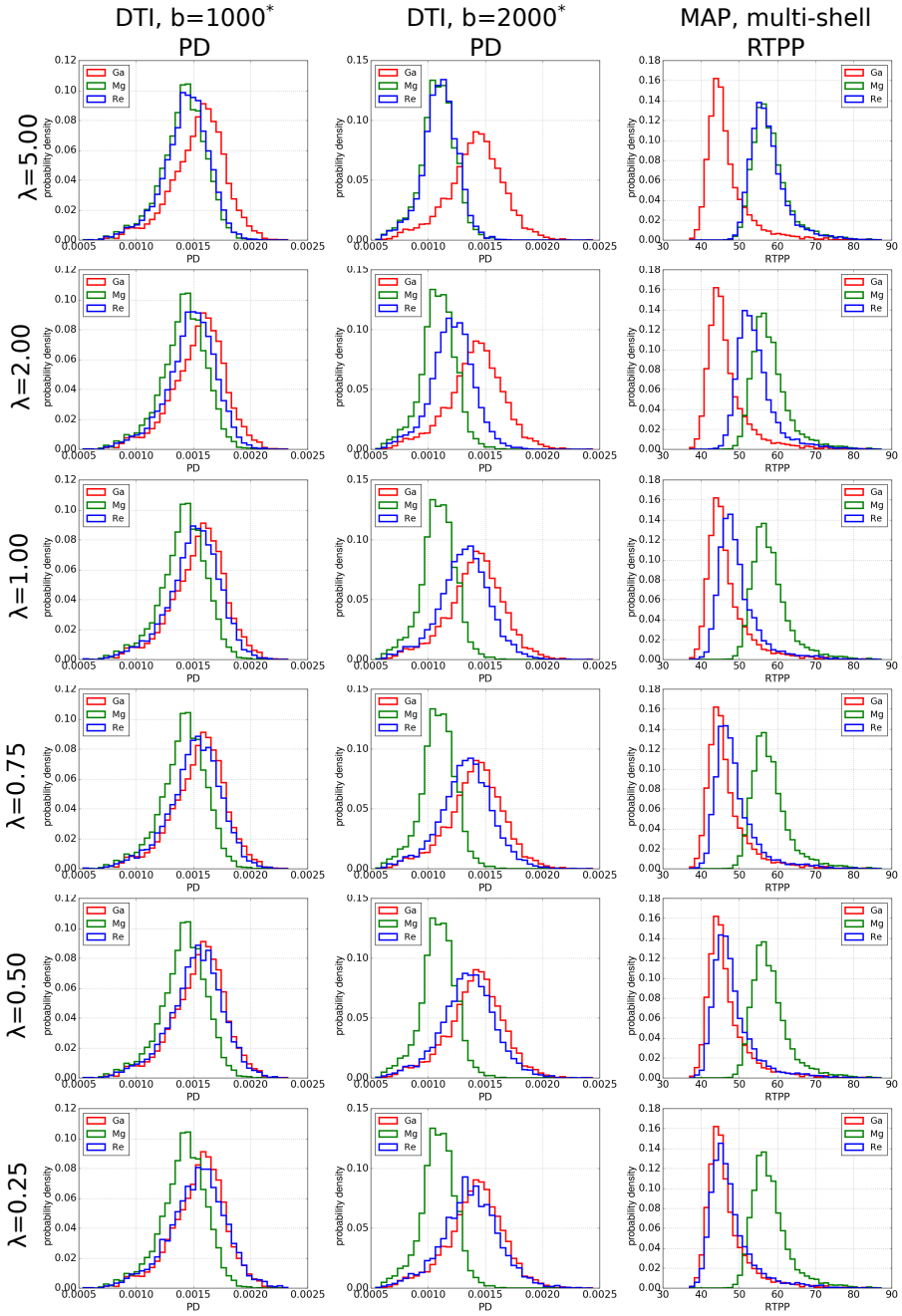

Fig. 4. Histograms of the principal diffusivity (PD) – for DTI at 1000, 2000 s/mm^2 – and return to plane probability (RTPP) – for MAP – estimated on Gaussian DWI ("Ga", red), Rician magnitude ("Mg", green) and phase-corrected real part ("Re", blue), $\mathrm{SNR}_0 = 10$. While the red and green histograms remain unchanged along the rows, the blue histograms change as function of the regularization parameter λ (see eq. (3)). As the attachment to the data decreases (from top to bottom) the phase-corrected histograms overlap more with the red Gaussian ones. *: s/mm^2.

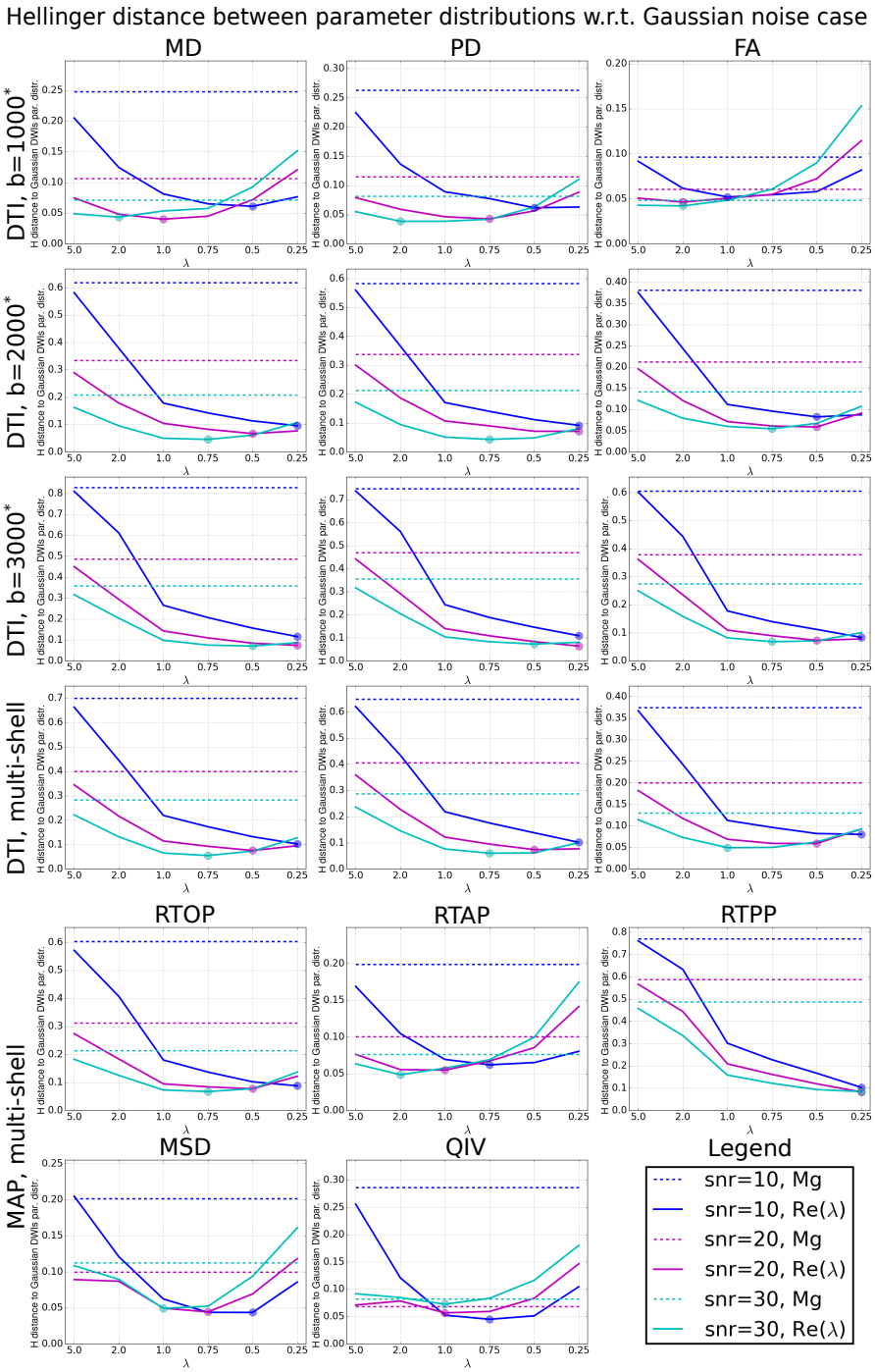

Fig. 5. Distance from Gaussianity (see eq. (6)) for DTI and q-space metrics calculated on Rician magnitude data ("Mg", dashed lines) and on phase-corrected real data ("Re", solid lines) as function of λ. The acquisition scheme changes for DTI in the first four rows. Each image reports color-encoded lines for different values of $\mathrm{SNR}_0 \in \{10, 20, 30\}$. The minimum distance for each solid line is highlighted by a dot. A lower value signifies more closeness to Gaussianity. *: s/mm^2.

restricted diffusion direction – which, in combination with a poor SNR_0, causes the effective SNR to fall well below 5 where a Rician distribution diverges from a Gaussian one. Therefore, the best λ value (highlighted with a dot in fig. 5) also depends on these factors. We point out that in some cases, as for DTI at $b = 1000\ s/mm^2$, too much filtering (small λ) causes the phase-corrected metric distributions to be more distant from Gaussianity compared to those based on the Rician magnitude (dashed lines). The best λ also seems to have a dependence on the considered metric. For instance, at $SNR_0 = 30$ the best λ for RTPP is 0.75 whereas for RTAP is 2. This can be associated to the fact that metrics that are highly related to signal measured along the less restricted diffusion direction, i.e. low intensity signal, such as PD and RTPP, benefit more than others of phase correction. See table 1 for a comprehensive summary.

Table 1. Maximum relative reduction $[0, 1]$ in H distance after phase correction compared to Rician magnitude (bias reduction). Values are reported for each acquisition type – $b = 1000$, 2000, 3000 s/mm^2 (1K,2K,3K), and multi-shell (ms) – and SNR_0.

SNR_0	MD (1K,2K,3K,ms)	PD (1K,2K,3K,ms)	FA (1K,2K,3K,ms)	RTOP ms	RTAP ms	RTPP ms	MSD ms	QIV ms
10	(.75,.84,.85,.85)	(.76,.84,.85,.84)	(.45,.78,.86,.78)	.85	.68	.86	.78	.84
20	(.62,.80,.84,.81)	(.63,.79,.86,.82)	(.24,.72,.86,.70)	.75	.45	.85	.55	.16
30	(.39,.78,.80,.80)	(.52,.80,.79,.79)	(.13,.61,.75,.62)	.68	.36	.82	.56	.11

4 Conclusion

We investigated the effects of phase correction of DWIs in terms of signal debiasing and Noise Floor removal. We quantitatively assess that phase correction has the potential of rendering nearly unbiased DTI and q-space metrics. Indeed, the noise distribution transformation, from Rician to Gaussian, allows compliance with the assumptions required to use standard least squares methods for signal estimation, avoiding noise floor related signal overestimation. In this work we illustrate the importance of accurate phase estimation of complex DWIs, necessary condition for a good phase correction. We plan to extend this work to other diffusion signal metrics, such as those derived from NODDI [5]. We believe that phase correction is still a challenging but promising tool for boosting the estimation of diffusion metrics.

Acknowledgments. Data for this project was provided by the MGH-USC Human Connectome Project. This work has received funding from the European Research Council (ERC) under the European Union's Horizon 2020 research and innovation program (ERC Advanced Grant agreement No 694665 : CoBCoM).

References

1. Jones, D. K., Basser, P. J.: "Squashing peanuts and smashing pumpkins": How noise distorts diffusion-weighted MR data. Magn. Reson. Med., 52(5), 979-993 (2004).

2. Aja-Fernández, S., Tristán-Vega, A.: A review on statistical noise models for Magnetic Resonance Imaging. LPI, ETSI Telecomunicacion, Universidad de Valladolid, Spain, Tech. Rep (2013).
3. Özarslan, E., Koay, C. G., Shepherd, T. M., Komlosh, M. E., İrfanoğlu, M. O., Pierpaoli, C., Basser, P. J.: Mean apparent propagator (MAP) MRI: a novel diffusion imaging method for mapping tissue microstructure. NeuroImage, 78, 16–32 (2013).
4. Alexander, D.C.: A general framework for experiment design in diffusion MRI and its application in measuring direct tissue-microstructure features. MRN, 60(2), 439–448 (2008).
5. Zhang, H., Schneider, T., Wheeler-Kingshott, C.A., Alexander, D.C.: NODDI: practical in vivo neurite orientation dispersion and density imaging of the human brain. Neuroimage, 61(4), 1000–1016 (2012).
6. Bernstein, M. A., Thomasson, D. M., Perman, W. H.: Improved detectability in low signal-to-noise ratio magnetic resonance images by means of a phase-corrected real reconstruction. Medical Physics, 16(5), 813-817 (1989).
7. Basser, P. J., Mattiello, J., LeBihan, D.: MR diffusion tensor spectroscopy and imaging. Biophysical journal, 66(1), 259–267 (1994).
8. Pizzolato, M., Ghosh, A., Boutelier, T., Deriche, R.: Magnitude and complex based diffusion signal reconstruction. In CDMRI, 127–140 (2014).
9. Liu, C., Bammer, R., Acar, B., Moseley, M. E.: Characterizing non-gaussian diffusion by using generalized diffusion tensors. Magn. Reson. Med., 51(5), 924-937 (2004).
10. Pizzolato, M., Wassermann, D., Boutelier, T., Deriche, R.: Exploiting the Phase in Diffusion MRI for Microstructure Recovery: Towards Axonal Tortuosity via Asymmetric Diffusion Processes. In MICCAI (2015).
11. Pizzolato, M., Wassermann, D., Duval, T., Campbell, J. S., Boutelier, T., Cohen-Adad, J., Deriche, R.: A Temperature Phantom to Probe the Ensemble Average Propagator Asymmetry: An In-Silico Study. In CDMRI, pp. 183–194 (2016).
12. Prah, D. E., Paulson, E. S., Nencka, A. S., Schmainda, K. M.: A simple method for rectified noise floor suppression: Phase-corrected real data reconstruction with application to diffusion-weighted imaging. Magn. Reson. Med., 64(2), 418–429 (2010).
13. Sprenger, T., Sperl, J. I., Fernandez, B., Haase, A., Menzel, M. I.: Real valued diffusion-weighted imaging using decorrelated phase filtering. Magn. Reson. Med., (2016).
14. Eichner, C., Cauley, S. F., Cohen-Adad, J., Möller, H. E., Turner, R., Setsompop, K., Wald, L. L.: Real diffusion-weighted MRI enabling true signal averaging and increased diffusion contrast. NeuroImage, 122, 373–384 (2015).
15. Caruyer, E., Daducci, A., Descoteaux, M., Houde, J.-C., Thiran J.-P., Verma, R.: Phantomas: a flexible software library to simulate diffusion MR phantoms. ISMRM14, (2014).
16. Caruyer, E., Lenglet, C., Sapiro, G., Deriche, R.: Design of multishell sampling schemes with uniform coverage in diffusion MRI. Magn. Reson. Med., 69(6), 1534–1540 (2013).
17. Fick, R. H., Wassermann, D., Caruyer, E., Deriche, R.: MAPL: Tissue microstructure estimation using Laplacian-regularized MAP-MRI and its application to HCP data. NeuroImage, 134, 365–385 (2016).
18. Hellinger, E.: Neue Begründung der Theorie quadratischer Formen von unendlichvielen Veränderlichen. J Reine Angew Math (1909).